GRAPH SLEPIANS TO STRIKE A BALANCE BETWEEN LOCAL AND GLOBAL NETWORK INTERACTIONS: APPLICATION TO FUNCTIONAL BRAIN IMAGING

Thomas AW Bolton[⋆†]*, Younes Farouj*[⋆†]*, Silvia Obertino*[‡]*, Dimitri Van De Ville*[⋆†]

[⋆] Institute of Bioengineering, École Polytechnique Federale de Lausanne (EPFL), Switzerland
[†] Department of Radiology and Medical Informatics, University of Geneva (UNIGE), Switzerland
[‡] Department of Computer Science, University of Verona (UNIVERO), Italy

ABSTRACT

Brain function exhibits coordinated activity patterns that are also reflected in anatomy, a finding that can be harnessed to constrain the dynamics of functional time series to the underlying structure while performing various signal processing operations. Graph signal processing (GSP) is such a framework, which we here equip with a new tool to uncover localised functional brain interactions. The functional magnetic resonance imaging (fMRI) signal is projected onto a collection of *Slepian vectors* defined on a graph extracted from structural and diffusion MRI data. This decomposition allows a multi-bandwidth description of signals that are maximally concentrated within a subset of nodes, as is often the case for neural activity. On simulated data, we compare this technique to classical Laplacian and localised Laplacian filtering. We then present, on real fMRI data, an illustration of the Slepians potential to retrieve localised interaction patterns in the context of a visual stimulation task.

***Index Terms*—** Graph signal processing, Slepians, Localised functional interactions

1 Introduction

Magnetic resonance imaging (MRI) has opened a number of avenues for the study of the brain. At the structural level, diffusion MRI enables to resolve the physical connectivity that exists between different regions. Viewed from the prism of graph analysis [1], this information is embedded in an adjacency matrix, which can then be decomposed into a set of canonical structural elements, commonly termed the *eigenmodes*.

In parallel, functional MRI (fMRI) offers a window on brain activity over time, and on its dynamics at rest or upon cognitive challenge. There is an exquisite relationship between brain function and the underlying structural scaffold [2]; for this reason, bimodal analytical approaches that can combine those two pieces of information are particularly tailored, and an emerging topic of interest.

In particular, graph signal processing (GSP) [3] has recently gained momentum for this purpose [4]. In this framework, functional information is regarded as temporal signals on a graph defined from structural measurements, and viewed as a linear combination of eigenmodes. This has the double advantage of enabling the study of structure/function relationships, and of permitting a wide set of signal processing operations in the spectral domain to improve the quality of functional signals.

In such approaches, a similar importance is typically assigned to each brain region (i.e., each node of the studied network) at the decomposition stage. However, in some settings, it may be desirable to enhance the accuracy of the analysis for a subset of particularly important areas (for example, the brain regions expected to respond to a given paradigm). At the same time, some flexibility is also desired when it comes to defining this subset, so that rough prior knowledge be enough information to provide.

Here, we demonstrate how this can be achieved through a generalised decomposition into Slepian vectors [5]. On simulated data, we observe that when provided with a set of nodes of interest, noisy functional signals can be recovered more accurately within this set compared to a standard decomposition. In addition, we show how error estimates are robust to changes in the selected subset. On real fMRI data, we exemplify the potential of Slepians to reveal subtler, localised interaction patterns in the context of a visual stimulation task.

2 Methods

2.1 Graph signal processing basics

Let a graph $\mathcal{G} = (\mathcal{V}, \mathbf{W})$ characterised by the set of N nodes $\mathcal{V}$, linked as described by the symmetrical adjacency matrix $\mathbf{W} \in \mathbb{R}^{N \times N}$. In the brain application considered here, $W_{i,j}$ will be large if brain regions i and j are strongly physically connected. The resulting Laplacian matrix admits an eigendecomposition as $\mathbf{L} = \mathbf{V}\mathbf{\Lambda}\mathbf{V}^\top$ [3], with $\mathbf{V} = [\mathbf{v_1}|\mathbf{v_2}|\dots|\mathbf{v_N}]$ containing the eigenmodes as its columns, arranged in ascending eigenvalue order $\lambda_1 < \lambda_2 < \dots < \lambda_N$. Because

$\lambda_k = \mathbf{v_k}^\top \mathbf{L} \mathbf{v_k} = \sum_{i \neq j} W_{i,j}([v_k]_i - [v_k]_j)^2$, eigenmodes of smaller eigenvalues will represent *low frequency* patterns on the graph, while eigenmodes of larger eigenvalues will denote less organised patterns with respect to the graph structure.

From this description, a signal $\mathbf{x} \in \mathbb{R}^{N \times 1}$ can conveniently be expressed in the graph domain as $\hat{\mathbf{x}} = \mathbf{V}^\top \mathbf{x}$, which is known as the *graph Fourier transform* (GFT) [6]; conversely, we also have $\mathbf{x} = \mathbf{V}\hat{\mathbf{x}}$. Each element of $\hat{\mathbf{x}}$ then represents the strength with which an eigenmode is contributing to the signal at hand.

In addition, note that the eigenmodes are also solutions to the Laplacian embedding problem, where the goal is to find a mapping of the graph nodes on a line so that connected ones stay as close as possible, that is, to find $\mathbf{x}$ as:

$$\mathbf{x}^* = \underset{\mathbf{x}}{\operatorname{argmin}}\, \mathbf{x}^\top \mathbf{L} \mathbf{x} = \underset{\mathbf{x}}{\operatorname{argmin}}\, \mathbf{x}^\top \mathbf{V} \mathbf{\Lambda} \mathbf{V}^\top \mathbf{x}, \qquad (1)$$

with $\mathbf{x}^\top \mathbf{x} = 1$ and $\mathbf{x}^\top \mathbf{1} = 0$ [7].

2.2 Graph Slepian vectors

The goal is to derive an alternative set of basis vectors, under the constraints that (1) their energy should be localised within a predefined subset of nodes $\mathcal{S}$, and (2) they should be derived from a bandwidth-limited subset of original eigenvectors, with dimension $K \leq N$ [8]. If we define the diagonal matrix $\mathbf{M}$ as $M_{i,i} = 1$ if $i \in \mathcal{S}$ and 0 otherwise, and $\mathbf{V_T} \in \mathbb{R}^{N \times K}$ as the trimmed set of eigenmodes, then the concentration to optimise is given by $\mu = \frac{\hat{\mathbf{x}}^\top \mathbf{C} \hat{\mathbf{x}}}{\hat{\mathbf{x}}^\top \hat{\mathbf{x}}}$, with $\mathbf{C} = \mathbf{V_T^\top M V_T}$.

For the analogy with classical eigenmodes, where λ_i represents a spatial frequency on the graph, we consider an alternative formulation for which, using the equality $\mathbf{\Lambda} = \mathbf{\Lambda}^{1/2} \mathbf{V}^\top \mathbf{V} \mathbf{\Lambda}^{1/2}$, the solution vectors $\mathbf{s_k}$, $k = 1, \ldots, K$ satisfy a generalised Laplacian embedding formulation [8]:

$$\hat{\mathbf{s}}^* = \underset{\hat{\mathbf{s}}}{\operatorname{argmin}}\, \hat{\mathbf{s}}^\top {\mathbf{\Lambda_T}}^{1/2} \mathbf{C} {\mathbf{\Lambda_T}}^{1/2} \hat{\mathbf{s}}, \qquad (2)$$

with $\mathbf{\Lambda_T} \in \mathbb{R}^{K \times K}$ the trimmed diagonal matrix of eigenvalues. The *local spatial frequency* within $\mathcal{S}$ is denoted ξ_i, and the matrix $\mathbf{S} = [\mathbf{s_1} | \mathbf{s_2} | \ldots | \mathbf{s_K}]$ contains the solution vectors, arranged in ascending frequency order ($\xi_1 < \xi_2 < \ldots < \xi_K$). Note that ξ_i will be low either if $\mathbf{s_i}$ is not concentrated within $\mathcal{S}$, or if it displays a low local spatial frequency.

2.3 Linear Slepian estimators

Let $\mathbf{X} \in \mathbb{R}^{N \times T}$ be a matrix of signals of length T defined on each of the N nodes of the graph. At any given time point t, the current signal value $\mathbf{X_t}$ can be projected onto the Slepian basis $\mathbf{S}$:

$$\mathbf{S}^\top \mathbf{X_t} = < \mathbf{X_t}, \mathbf{s_i} >_{i=1,\ldots,K} . \qquad (3)$$

Now, assuming that $\mathbf{X_t}$ is composed of a smooth component (i.e., the signal of interest) and of a noise component of larger frequency, it is possible to truncate the projection without loss of information, by discarding the Slepian coefficients associated to the largest ξ_i. At the same time, one can also focus on $\mathcal{S}$ by discarding non-concentrated Slepian vectors ($\mu_i < \epsilon$). Formally, we retrieve the output $\mathbf{Y_t^{(\bar{\xi})}} \in \mathbb{R}^{N \times 1}$ as:

$$\mathbf{Y_t^{(\bar{\xi})}} = \mathbf{S} \mathbf{H}^{(\bar{\xi})} \mathbf{S}^\top \mathbf{X_t}, \qquad (4)$$

where $\bar{\xi}$ is the cut-off frequency and $\mathbf{H}^{(\bar{\xi})}$ is a diagonal matrix with $H_{i,i}^{(\bar{\xi})} = 1$ if $\xi_i < \bar{\xi}$ and $\mu_i > \epsilon$, and 0 otherwise. We call this estimator *linear* in analogy with classical estimators on regular domains (DCT [9], wavelets [10]), as it depends only on the cut-off frequency and does not involve any point-wise thresholding procedure.

2.4 Evaluations on simulated data

We examined how well a simulated ground truth signal $\mathbf{X} \in \mathbb{R}^{N \times T}$ on $\mathcal{G}$, corrupted with noise, could be retrieved on a subset of nodes $\mathcal{S}$ through graph filtering. We considered simulated modular graphs [11] of $N = 200$ nodes generated with the *Graph Signal Processing* toolbox [12], which had 4 communities, a minimal community number of 40 nodes, and world density $\frac{1}{N}$. We created simulated time courses of $T = 900$ time points, where the largest graph community was selected as $\mathcal{S}$. Within $\mathcal{S}$, we designed two independent temporal paradigms of 180 time points, each occurring in a randomly selected half of the subset nodes. Each of the other 3 communities was also assigned a separate paradigm time course (see Figure 1A).

At each time point, a random subset of n_r nodes was chosen, and corrupted with noise of intensity $I \sim \mathcal{N}(0, \sigma_r^2)$ (see Figure 1B). We assessed the ability of (1) a classical basis of eigenmodes (GFT), (2) a localised eigenmodes decomposition on the subset $\mathcal{S}$ (LGFT), and (3) a Slepian basis focused on the same subset (SLEP) to retrieve the ground truth. We probed ranges of $n_r \in [0 : 20 : 200]$ and $\sigma_r \in [0 : 0.5 : 4]$, simulating 20 datasets in each case. We computed the average mean squared error (MSE) across all nodes within $\mathcal{S}$ for all possible filtering cutoffs, and selected the minimal MSE as our error measure. In addition, we also compared the LGFT and SLEP decompositions in their sensitivity to an imperfect subset selection, where for each simulated dataset, a random $\mathcal{S}_i$ ($|\mathcal{S}_i| = 0.2|\mathcal{S}|$) was picked 10 separate times as the subset of interest.

2.5 Exploratory application to real fMRI data

To extend our observations on simulated data to the fMRI setting, we considered one subject (ID:100307) from the Human Connectome Project initiative [13], for which we downloaded diffusion MRI, structural MRI and task fMRI (*Working Memory*) data. We created $\mathbf{W}$ from the structural and diffusion data, using the *MRtrix* toolbox [14] (multi-shell multi-tissue response function estimation, spherical deconvolution,

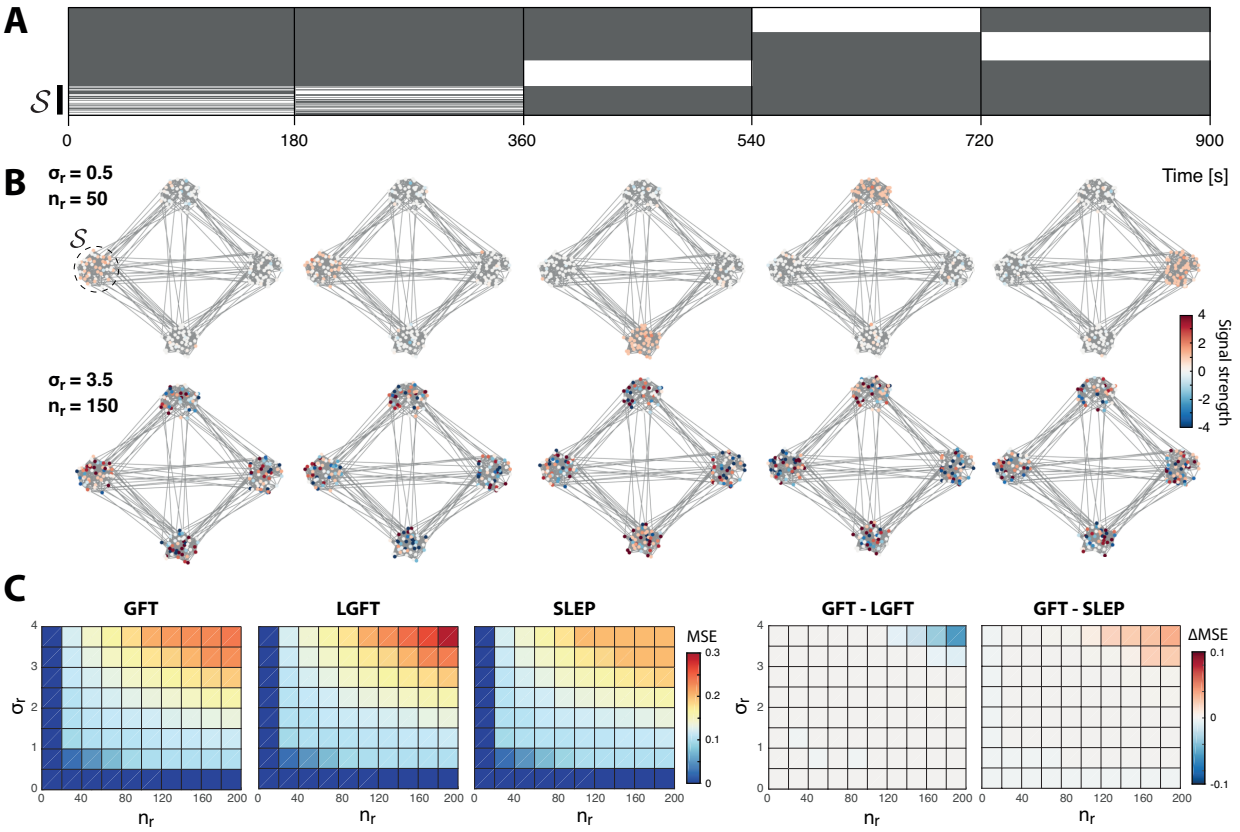

Fig. 1. (A) Simulated paradigm for all nodes (top to bottom) across time (left to right). White denotes activation, and $\mathcal{S}$ reflects the selected subset. (B) In low noise (top) or high noise (bottom) cases, example signals generated at different moments from the paradigm, on a simulated graph. (C) For GFT, LGFT or SLEP cases, evolution of median MSE across simulated datasets for increasing noise levels, and difference in median MSE between GFT and LGFT, or GFT and SLEP approaches.

tractogram generation with 10^7 output streamlines between $N = 838$ regions from the Craddock atlas [15]).

The considered working memory task fMRI recording ($TR = 0.72s$, $T = 395$ scans) included blocks of fixation, and of image presentation (faces, places, tools or body parts), in 0-back or 2-back fashion [16]. Here, we focused on the visual aspect of the paradigm, and selected a subset $\mathcal{S}$ of $|\mathcal{S}| = 3$ areas from the occipital brain (see Figure 2A). We generated Slepian coefficients at a bandwidth $K = 180$, and truncated them with $\epsilon = 10^{-2}$, yielding 2 remaining coefficients at each time point. We compared this two-dimensional representation of functional brain activity to the one achieved from the coefficients of the 2 GFT or LGFT eigenmodes of lowest frequency.

3 Results

3.1 Evaluations on simulated data

Across trials, MSE increased with larger n_r and larger σ_r, for all three evaluated methods (GFT, LGFT, SLEP; Figure 1C). Performance was equivalent at low noise levels, but in the noisiest cases (top right part of the matrices), a better ground truth recovery was achieved with Slepians. For instance, for $n_r = 200$ and $\sigma_r = 4$, median MSE values were $MSE_{GFT} = 0.26$, $MSE_{LGFT} = 0.36$, and $MSE_{SLEP} = 0.2$.

In addition, the LGFT approach was less robust than the SLEP one to an incomplete $\mathcal{S}$ selection: for example, at still moderate noise levels of $n_r = 100$ and $\sigma_r = 2$, median MSE in the LGFT case was 0.29 (compared to 0.13 for a full subset selection), whereas it stayed at 0.14 in the SLEP case (against 0.13 for a full subset selection).

3.2 Exploratory application to real fMRI data

Plotting the spectral coefficients linked to the 2 lowest frequency GFT eigenmodes (Figure 2B, left plot), no clear discrimination could be achieved between the moments when different types of visual stimuli were presented. In the LGFT case (middle plot), moments of fixation (dark blue) could be segregated from visual presentation. In the SLEP case (right

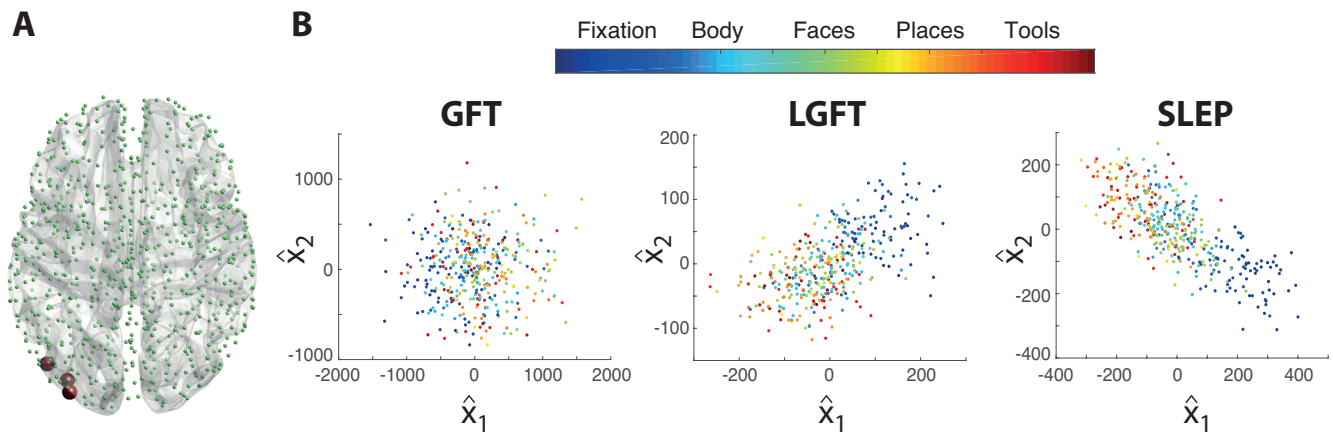

Fig. 2. (A) Brain depiction of the considered set of nodes, with the selected subset $\mathcal{S}$ highlighted in red. (B) For the GFT (left), LGFT (middle) and SLEP (right) cases, evolution over time of the signal projected on the two lowest frequency eigenmodes/Slepian vectors. Colour coding reflects the type of stimulus presented at each time point (note that the paradigm regressor was convolved with a hemodynamic response function estimate, using SPM12 (http://www.fil.ion.ucl.ac.uk/spm/), to retrieve an fMRI-compatible timing).

plot), on top of distinguishing fixation from visual presentation, the presentation of body parts or faces (light blue or green data points) could be separated from moments when places or tools (orange or red data points) were shown.

4 Discussion

In this work, we compared traditional GSP tools relying on a decomposition into brain eigenmodes to a generalised Slepian approach. For simulated data partitioned into communities, as is known to occur in functional neuroimaging [17], we showed that retrieval of ground truth activity patterns on a selected subset of nodes would be more largely impeded by noise in the case of global (GFT) or local (LGFT) decompositions into eigenmodes, as compared to a Slepian-based approach. This was, in particular, observed for large noise levels: in the LGFT case, the decomposition includes a lower amount of eigenmodes (equal to the number of subset nodes), which complicates the disentanglement between noise and signal of interest. In the GFT case, the complex structure of the noise at hand degrades the estimates more than when using Slepian vectors, which are linear combinations of eigenmodes localised within the subset of interest; by retaining only those satisfying $\mu_i > \epsilon$ (that is, the most locally concentrated ones), a large fraction of the noise (which spans the whole network) is eliminated, resulting in a more accurate ground truth retrieval. Computationally speaking, note that another asset of Slepians is the possibility to rapidly recompute them for other bandwidth or node subset settings following the initial decomposition into eigenmodes (indeed, as seen in Equation (2), the problem then boils down to the eigendecomposition of $\mathbf{\Lambda_T}^{1/2}\mathbf{C}\mathbf{\Lambda_T}^{1/2}$, which has size $K \times K$, and subsequent inverse GFT of Slepian coefficients).

At the same time, we saw that a decomposition into Slepian vectors offered more robustness to an imperfect selection of nodes: compared to the LGFT case where MSE strongly rose, estimates in this first setting remained almost similar, despite focusing the analysis on a subset with only 20% of nodes of interest. This is enabled by the additional bandwidth parameter, thanks to which Slepian vectors can also cover nodes outside the selected subset, following the relationships embedded in $\mathbf{W}$. In fact, there are two separate possible benefits: first, the robustness to imperfect node selection as we report here, and second, the possibility for Slepian vectors to also embed information about *non-trivial* interacting partners, if they are linked to some nodes of $\mathcal{S}$ in $\mathbf{W}$. Given those specificities, it is perhaps unsurprising that on an exploratory application to fMRI data, a projection of the signal onto Slepian vectors enabled the best discrimination between paradigm subtypes, despite the very low amount of nodes that constituted the subset of interest.

From a neuroscience perspective, analyses based on Slepians thus consist in an interesting way to combine imaging modalities, as structural connectivity (i.e., $\mathbf{W}$) informs the decomposition of functional signals (i.e., $\mathbf{X}$). In future work, it will be interesting to apply this framework to an extended battery of fMRI recordings, to assess the consistency of its merits across subjects and task paradigms. Further, a simple, yet powerful extension could be achieved by forcing Slepian vectors not only to be maximally concentrated within a subset $\mathcal{S}_1$, but also to be *minimally concentrated* within another subset $\mathcal{S}_2$; this is easily done by enabling $M_{i,i}$ to take a value of -1 for nodes falling in the latter subset.

5 References

[1] Y Iturria-Medina, EJ Canales-Rodriguez, L Melie-Garcia, PA Valdes-Hernandez, E Martinez-Montes, Y Alemán-Gómez, and JM Sánchez-Bornot, "Characterizing brain anatomical connections using diffusion weighted MRI and graph theory," *Neuroimage*, vol. 36, no. 3, pp. 645–660, 2007.

[2] Ed Bullmore and Olaf Sporns, "Complex brain networks: graph theoretical analysis of structural and functional systems," *Nature reviews. Neuroscience*, vol. 10, no. 3, pp. 186, 2009.

[3] David I Shuman, Sunil K Narang, Pascal Frossard, Antonio Ortega, and Pierre Vandergheynst, "The emerging field of signal processing on graphs: Extending high-dimensional data analysis to networks and other irregular domains," *IEEE Signal Processing Magazine*, vol. 30, no. 3, pp. 83–98, 2013.

[4] Weiyu Huang, Leah Goldsberry, Nicholas F Wymbs, Scott T Grafton, Danielle S Bassett, and Alejandro Ribeiro, "Graph frequency analysis of brain signals," *IEEE Journal of Selected Topics in Signal Processing*, vol. 10, no. 7, pp. 1189–1203, 2016.

[5] David Slepian and Henry O Pollak, "Prolate spheroidal wave functions, Fourier analysis and uncertainty," *Bell Labs Technical Journal*, vol. 40, no. 1, pp. 43–63, 1961.

[6] Aliaksei Sandryhaila and José MF Moura, "Discrete signal processing on graphs," *IEEE transactions on signal processing*, vol. 61, no. 7, pp. 1644–1656, 2013.

[7] Mikhail Belkin and Partha Niyogi, "Laplacian eigenmaps for dimensionality reduction and data representation," *Neural computation*, vol. 15, no. 6, pp. 1373–1396, 2003.

[8] Dimitri Van De Ville, Robin Demesmaeker, and Maria Giulia Preti, "When Slepian Meets Fiedler: Putting a Focus on the Graph Spectrum," *IEEE Signal Processing Letters*, vol. 24, no. 7, pp. 1001–1004, 2017.

[9] Leonid P Yaroslavsky, Karen O Egiazarian, and Jaakko T Astola, "Transform domain image restoration methods: review, comparison, and interpretation," in *Photonics West 2001-Electronic Imaging*. International Society for Optics and Photonics, 2001, pp. 155–169.

[10] David L Donoho and Jain M Johnstone, "Ideal spatial adaptation by wavelet shrinkage," *biometrika*, vol. 81, no. 3, pp. 425–455, 1994.

[11] Santo Fortunato and Darko Hric, "Community detection in networks: A user guide," *Physics Reports*, vol. 659, pp. 1–44, 2016.

[12] Nathanaël Perraudin, Johan Paratte, David Shuman, Lionel Martin, Vassilis Kalofolias, Pierre Vandergheynst, and David K. Hammond, "GSPBOX: A toolbox for signal processing on graphs," *ArXiv e-prints*, Aug. 2014.

[13] David C Van Essen, Stephen M Smith, Deanna M Barch, Timothy EJ Behrens, Essa Yacoub, Kamil Ugurbil, Wu-Minn HCP Consortium, et al., "The WU-Minn human connectome project: an overview," *Neuroimage*, vol. 80, pp. 62–79, 2013.

[14] J Tournier, Fernando Calamante, Alan Connelly, et al., "MRtrix: diffusion tractography in crossing fiber regions," *International Journal of Imaging Systems and Technology*, vol. 22, no. 1, pp. 53–66, 2012.

[15] R Cameron Craddock, G Andrew James, Paul E Holtzheimer, Xiaoping P Hu, and Helen S Mayberg, "A whole brain fMRI atlas generated via spatially constrained spectral clustering," *Human brain mapping*, vol. 33, no. 8, pp. 1914–1928, 2012.

[16] Deanna M Barch, Gregory C Burgess, Michael P Harms, Steven E Petersen, Bradley L Schlaggar, Maurizio Corbetta, Matthew F Glasser, Sandra Curtiss, Sachin Dixit, Cindy Feldt, et al., "Function in the human connectome: task-fMRI and individual differences in behavior," *Neuroimage*, vol. 80, pp. 169–189, 2013.

[17] Jonathan D Power, Alexander L Cohen, Steven M Nelson, Gagan S Wig, Kelly Anne Barnes, Jessica A Church, Alecia C Vogel, Timothy O Laumann, Fran M Miezin, Bradley L Schlaggar, et al., "Functional network organization of the human brain," *Neuron*, vol. 72, no. 4, pp. 665–678, 2011.